Technical Sciences
Academy of Romania
www.jesi.astr.ro

Journal of Engineering Sciences and Innovation
Volume 11, Issue 1 / 2026, 71 - 84

C. Chemical Engineering, Materials Science and Engineering

Received ***5 August 2025*** *Accepted* ***11 March 2026***
Received in revised form ***24 January 2026***

Special mechanical properties of diboride ceramic composites with complex microstructures: comparative analysis of three study cases

BADICA PETRE[1*], GRIGOROSCUTA MIHAI-ALEXANDRU[1], KUNCSER ANDREI[1], BURDUSEL MIHAIL[1], ALDICA GHEORGHE[1], VASYLKIV OLEG[2]

[1]National Institute of Materials Physics, Atomistilor str. 405A, Magurele 077125, Romania
[2]National Institute for Materials Science, 1-2-1 Sengen, Tsukuba, Ibaraki 305-0047, Japan

Abstract. Ceramics are hard and brittle materials. They are usually difficult to machine by chipping due to a strength-ductility trade-off. Moreover, their strength decreases at high temperatures. In this work, we review the peculiar features of three systems with unique mechanical properties. The MgB_2 added with hBN (hexagonal BN) and G (graphene) is machinable by chipping and is assessed for bulk superconducting magnets. The second system is a TiB_2-B_4C structural ceramic composite (70/30 vol.) with a high bending strength of 1.1 GPa at 1800°C, showing an unusual shape of the bending strength–strain curve composed of elastic, ductile, and strengthening regions. The third system is the heterogeneous, multiphase high-entropy diboride $(Ti_{0.25}Ta_{0.25}Hf_{0.25}Zr_{0.25})B_2$. Remarkably, it demonstrates a deformation-resistant mechanism that persists with increasing temperature up to 1800°C. Ductile behavior (7.5% strain) is observed at 2000°C, while the bending strength (407 MPa) is 25% higher than at room temperature.

Keywords: diborides, composites, high entropy materials, strangth-ductility trade-off, microstructure, superconductor.

1. Introduction

Mechanical properties of materials are crucial for their use in any field of human activity. There is continuous pressure from society for improved and controlled properties. Industries such as automobile, aerospace, power, energy, and others demand high-strength materials. These materials should also have low density, which helps achieve higher efficiency, portability, flexibility, integration, and

[*]Correspondence address: badica2003@yahoo.com, petre.badica@infim.ro

miniaturization, as well as lower carbon emissions. This enables the design and fabrication of new, innovative devices and systems. They should also have good ductility and toughness for forming into various shapes and for preventing catastrophic failure of components during service. Moreover, materials should operate under special or extreme conditions of temperature, pressure, field gradient, or in corrosive/oxidation environments.

The current market of structural materials is dominated by alloys such as steels, nickel-based superalloys, aluminum, and titanium alloys. They show different drawbacks, and we mention some of them: (i) An increase in strength is often obtained for a higher density [1]; (ii) The strength of Al alloys, Ti alloys, and Ni-based alloys is usually stable up to service temperatures of ~473, 800, and 1100 °C, respectively. At higher operating temperatures, these alloys present a deterioration of the mechanical properties due to temperature-dependent effects, e.g. grains coarsening, interfaces modification, and diffusion; (iii) Another undesirable trend is that strength and ductility are mutually exclusive mechanical properties: this paradigm is known as the strength-ductility trade-off and it indicates that materials can be either strong or ductile, but rarely both at the same time [2-5]. Improvement of indicated alloys as well as search for new high-performance high-temperature alloys such as Mo, W, Ta, or Nb ones [6] are among the very active topics of research in the field of structural materials science and engineering. Literature also indicates other candidates such as eutectic [1] and high entropy [7-10] alloys and metal-matrix composites. By broadening the classical meaning of composites, Sathiyamoorthi and Kim review the metal-based heterogeneous systems [11] where the defining terms used are ‘hierarchical’, ‘multimodal’, ‘gradient’ structures and these materials show a different and improved strength-ductility trade-off behavior comparative to homogeneous systems.

Of much interest are also other heterogeneous systems, and it is worthy to note that components can be organic, metal, ceramic, or complex units (e.g., eutectics, solid solutions), and these systems, due to complex organization, hierarchical or not, may overcome the challenges of the strength-ductility limitations [12]. Geonics and bioionics, the science of constructing artificial systems that borrow some of the characteristics of geological and of living systems, respectively [13] are introduced and used in designing new materials with outstanding properties. Materials available in nature such as minerals, mollusk and turtle shells, fish scales and pearls, osteodermal plates and ivory horns, wood and bamboo, and others are, in many cases, mechanically superior to artificial ones. To achieve high performance, i.e. to accomplish one or more characteristic(s)/function(s) in an optimum manner, heterogeneous materials take advantage in a synergetic manner of the components with a certain chemical composition, crystal structure, defects, strain, anisotropy, size, size distribution, morphology, etc., and of their arrangement and interaction creating different patterns. This synergy principle in heterogeneous material systems also successfully applies to other properties than the mechanical ones. In such systems, it is possible to induce or enhance electronic, spintronic, and other properties not available or attained by components alone. This opens interesting

novel possibilities to combine and control multiple functionalities in a heterogeneous system. Although patterns are linked and depend on structure/microstructure, it is necessary to make a distinction between the microstructural patterns (morphology, composition, etc.) that are independent on the excitation and patterns that are dependent on excitation, e.g. on application of the mechanical load. In the second category are patterns of e.g. strain gradients and distribution, and of defects formation and evolution. The patterns including the microstructural ones are generated on one or more dimensional scales, from nano to micro and to macro.

Indeed the microstructures of the already mentioned materials from nature show this feature, i.e. their microstructure is complex with a specific level of organization at one or at multiple dimensional scales [13-15]. Mimetic approaches to obtain artificial heterogeneous materials similar to those from nature seems attractive, but a key issue is that many natural materials of interest are obtained within long periods of time, by complex physical-chemical-biological processes and often require peculiar and complex synthesis conditions. Therefore, in practice it is necessary to look for heterogeneous materials designs that can be easily fabricated with available and preferably cheap technologies and within a reasonable time. This requirement also questions the necessity of materials with extremely high number of elements and components decreasing reproducibility and industrialization potential.

In this work we compare three ceramic materials with peculiar mechanical properties. They overcome to some extent the strength-ductility trade off. They show microstructures with specific features at different scales. Some aspects shared by these systems as well as those open for discussion and future research are introduced. The first system is the MgB_2 superconductor. It has a critical temperature T_c of 39 K [16] meaning that it can be used e.g. at liquid hydrogen temperatures, thus being compatible with envisioned clean and sustainable future hydrogen economy. MgB_2 has the lightest weight (2.63 g/cm^3) among practical superconductors, it is free of rare earth and precious metals and it is bio- and eco-compatible [17]. Mechanically it is has a relatively high strength, but its ductility is low, being brittle. This makes difficult its machining by chipping for fabrication of parts with desired shapes. To provide forming by machining, MgB_2-based composites were obtained by adding hBN (hexagonal BN) and G (graphene) [18, 19]. A small amount of other additives were added to influence superconducting characteristics, namely trapped magnetic field, B_{tr} [20] Trapped magnetic field defines the potential of using the material as a superconducting magnet and higher values are desired. Second system is the TiB_2-B_4C ceramic composite (70/30 vol. %). It has a high bending strength of ~1.1 GPa at 1800 °C. The shape of the bending strength–strain curve at high temperature is unusual being composed of a region with a typical elastic behavior, followed by two regions where elastic and plastic deformation components are simultaneously active and contribute with a different weight leading to strengthening and ductile behaviors [21]. Finally, the high-entropy diboride $Ti_{0.25}Ta_{0.25}Hf_{0.25}Zr_{0.25})B_2$ obtained from a mixture of diboride

powders is considered [22]. The material is a composite with Ta-rich/Ti-poor (reinforcement) and Ta-poor/Ti-rich (matrix) complex diboride grains. At nanoscale, the grains are heterogeneous, being composed of regions with a multitude of complex diboride compositions. Presented microstructural features at nano- and microscales enable use of the term 'heterogeneous multiphase high entropy diboride' and they are considered the reason for the noted extraordinary mechanical properties. Namely, under bending load, a deformation-resistant mechanism occurs with the increase of temperature. A strengthening process increases the room temperature (RT) bending strength (326 MPa) by ≈50% at 1800 °C (488 MPa). At 2000 °C a ductile behavior with a deformation strain of ~7.5% occurs, while bending strength (407 MPa) is ~25% above the value at RT.

2. Experimental

2.1 Sample preparation

Materials were obtained by powder metallurgy. Raw powders were MgB_2, TiB_2, TaB_2, HfB_2, ZrB_2, hexagonal BN (h-BN), graphene (G), Te and B_4C. They were mixed to obtain the following compositions: $MgB_2(h\text{-}BN)_{0.01}$+10 wt.% h-BN ($MgB_2$-hBN), $MgB_2(Te)_{0.01}$+10 wt.% h-BN (MgB_2-hBN-Te), $MgB_2(G)_{0.01}$+10 wt.% G (MgB_2-G), $MgB_2(B_4C)_{0.01}$+10 wt.% G (MgB_2-G-B_4C), TiB_2-B_4C (70/30 vol.%), and $Ti_{0.25}Ta_{0.25}Hf_{0.25}Zr_{0.25})B_2$. Powder mixtures we processed by spark plasma sintering (SPS). The MgB_2- based samples were fabricated with a FCT Systeme GmbH HP D5 (Germany) equipment at at 1150 °C for 3 min. The other two bulk systems were also obtained by SPS, but by using a furnace 'Dr. Sinter' 1050 from Sumitomo (Japan). Sintering conditions of TiB_2-B_4C and $Ti_{0.25}Ta_{0.25}Hf_{0.25}Zr_{0.25})B_2$ were 1900 °C for 10 min and 1927 °C for 20 min, respectively. Details on raw materials, sample preparation as well as on sample characterization from Section 2.2 are given in refs. [20-22].

2.2 Sample characterization

Microstructure of the samples was observed by secondary electron microscopy (SEM) and transmission electron microscopy TEM by using Tescan Lyra 3XMU and JEOL 2100, respectively.

Forming of the bulks into different shapes was performed through machining by chipping using lathe and milling machines. Three-point bending tests at different temperatures were conducted with a Shimadzu AG-X plus system on bars cut from SPSed disks (h × w × l = 2 mm × 2.3 mm × 20 mm) for a span of 16 mm. Loading speed was 0.5 mm/min.

A Hall sensor (LHP-MU by AREPOC s.r.o, Slovakia) was placed on the top surface of the SPSed MgB_2-based disk, at the center. Trapped magnetic field B_{tr} was measured in a PPMS (Quantum Design 14 T) magnet. At 40 K that is above the critical temperature, a magnetic field of 5 T was applied and sample was field

cooled down to 12 K. After stabilization, applied field B_{app} is decreased with a constant rate of 0.00015 T/s down to − 5 T. At this rate, we found that occurrence of undesirable macro-flux jumps is avoided.

3. Results and Discussion

3.1 Machinable by chipping MgB_2 superconductor for bulk superconducting magnet applications

MgB_2 becomes machinable by chipping for minimum ~8 wt. % additive, hBN or G [18,19]. The microstructure of the composite (10 wt. % additive) indicates the presence of two interpenetrated 3D networks [12] formed by MgB_2 and hBN or G additives [20]. Namely, there are grains and regions of the MgB_2 phase and of the additive that are interconnected extending from the hundreds of nanometers to about tens of microns. This microstructure allows percolative supercurrent flow over the entire sample, providing the background for energy storage as a superconducting diamagnetic magnet. Distribution of the phases impact both mechanical properties and superconducting characteristics.

In the case of mechanical properties, selected additives and processing conditions allow to a large extent to preserve the integrity of MgB_2, hBN and G [23, 24] phases since chemical reactions between the superconductor and the additives has been limited. While MgB_2 is relatively hard and brittle, hBN and G are soft and can be mechanically exfoliated because their hexagonal crystal structure is composed of atom layers connected by weak Van der Waals bonding. We note that MgB_2 has also a hexagonal layered crystal structure (Hermann-Mauguin space group P6/mmm typical of AlB_2). In this case, layers of Mg and B alternate and between the layers, Van der Waals bondings are active. The MgB_2 crystal structure is shared by the diborides TiB_2, TaB_2, HfB_2, ZrB_2 and the high entropy diboride (HEDB) $(Ti_{0.25}Ta_{0.25}Hf_{0.25}Zr_{0.25})B_2$ addressed in Sections 3.2 and 3.3. One observes that hBN, G and diborides have similar features of crystal chemistry, but there are also differences especially related to bonding strength, in plane and out of plane. The differences are important for designing and control of tailored mechanical properties. For MgB_2-hBN or MgB_2-G superconducting composites, softer hBN and G phases initiate machining by chipping and also confine the brittle MgB_2 micro regions which are removed by pull out and comminution due to their more brittle character when in contact with a hard cutting tool. Soft regions also act as absorbers of fractures leading to cracks-free parts with desired shapes (Fig. 1).

Minor additives were not observed to significantly impact machinable characteristics of the composites added with hBN or G, but they can improve superconducting properties leading to enhancement of the B_{tr}. For example, introduction of minor additives Te and B_4C in MgB_2-hBN and MgB_2-G compositions, respectively, promote values of $B_{tr,}{}^{max}$ and $B_{tr}{}^{0T}$ of 3.48 and 1.84 T, 2.73 and 2.16 T versus 3.28 and 1.75 T, 2.6 and 2.07 T in samples without minor additives (Fig. 2). Minor additives provide nano-precipitates (e.g. MgTe) or are

acting as sources of carbon (e.g. B_4C) for boron substitution in the crystal lattice of MgB_2. In both cases, connectivity and pinning centers directly or indirectly are influenced by the minor additives use, resulting in improvement of B_{tr}.
This section provides arguments that wise microstructural control at nano and micro scales can be rewarding. The MgB_2 gains two essential features that are acting simultaneously: the material retains and improves its superconducting characteristics, while it becomes machinable by chipping so that mechanical strength keeps a convenient level for superconducting bulk magnet and other applications.

(a) (b) (c)

Fig. 1 (a)- MgB_2 machinable cylinder drilled on a lathe machine and longitudinally cut to observe the shape and precision of the cut; (b) – spiral made of machinable MgB_2 obtained on a milling machine; (c) concentric rings obtained by mechanical processing on a milling machine (followed by polishing).

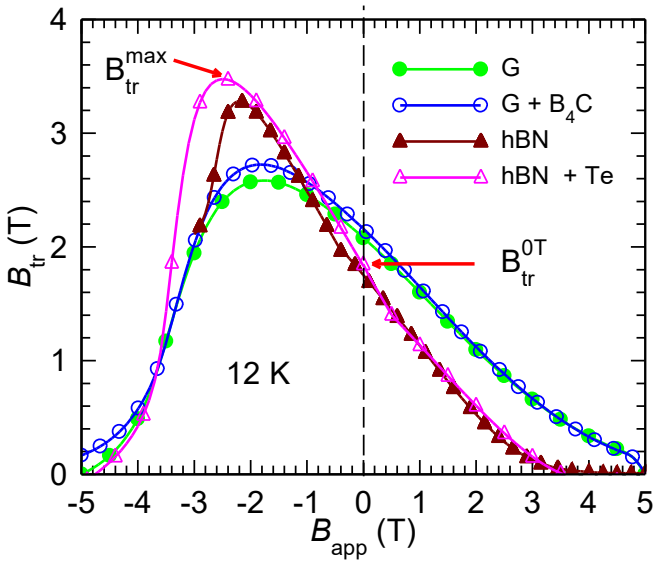

Fig. 2 Trapped magnetic field B_{tr} measured at 12 K vs. applied magnetic field B_{app} for samples MgB_2-hBN, MgB_2-G, MgB_2-hBN-Te and MgB_2-G-B_4C. Measurement was performed in field-cooling arrangement for a B_{app} decrease rate (from +5T to -5T) of 0.00015 T/s. The B_{app} decrease rate was selected to avoid thermomagnetic instabilities such as undesirable flux jumps.

3.2 Strenghtening and ductility at 1800°C in TiB_2-B_4C composite

The TiB_2-B_4C composite has according to definitions from ref [12] a 3D interpenetrated microstructure. It is interesting to observe that this type of microstructure was also observed in the case of MgB_2-hBN and MgB_2-G composites (see Section 3.1). At room temperature and at 1600 °C the TiB_2-B_4C composite under bending load shows typical elastic behavior with a brittle fracture and limited or no plasticity. With the increase of temperature, elastic modulus shows a small variation, while fracture strain increases slightly being below 0.6 %. At 1800 °C, material has a peculiar behavior (Fig. 3). There is an elastic region as for lower temperatures with similar elastic modulus and a strain of 0.6-0.8 % (region A). But, at the end of elastic region, material does not collapse and, surprisingly, it develops a plastic region for almost a constant bending strength (around 250 MPa) up to strains of ~12 % (region B). Beyond this strain, there is a strengthening region (region C), which is almost linear, i.e., appears to have an elastic character. In this strengthening region, the material reaches a high bending strength of over 1.1 GPa.

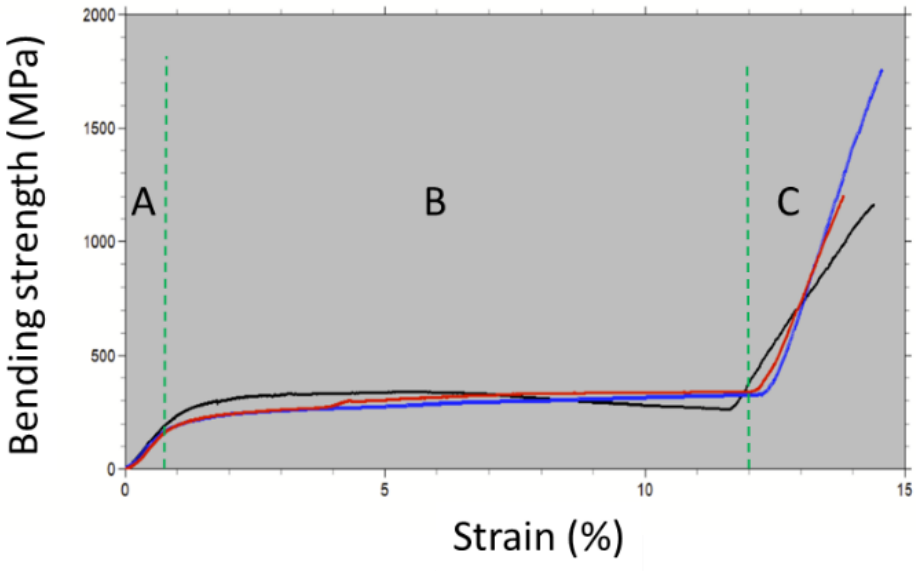

Fig. 3. Bending strength-stress curves on TiB_2-B_4C composite (3 samples).

Observation by SEM of the microstructure after bending at 1800 °C at the micron level could not present evidence for a special fracturing mechanism explaining the complex shape of the strength-strain curves. Nanoscale details revealed with TEM provided some insight. It was found that B_4C grains play a major role in the extraordinary ductility-strengthening behavior and can explain specifics of the bending strength curves. By comparing the fractured and free-ends areas of the

sample after bending at 1800 °C we noticed that stacking faults with (1-11) and (011) stacking planes and twins with (1-11) twinning plane rearrange into nano-twins with (10-1) twinning planes, orthogonal, but equivalent to the initial ones. The proposed reorganization mechanism of the defects runs as follows [21]: An external force, of bending in this case, when applied along the (1-11) twinning planes activates stacking faults (stage I) and may force the twinned domains to rotate and align (stage II). As the deformation on one direction (i.e. along the twinning planes) is constrained by the external applied force and it is also influenced by B_4C-B_4C or TiB_2-BC grain boundaries and defects in B_4C that may oppose sliding, due to energy dissipation reasons, a shearing on orthogonal direction emerges (stage III), thus being active especially along the (011) stacking faults which are more susceptible to crystallographic rearrangement. An energetically stable state is attained in the system when the shearing provides enough energy for the crystal structure to be rearranged into new nano twins (stage IV) with (10-1) twinning planes (Fig. 4).

The bending strength-strain curves from Fig. 3 are interpreted by applying the defects rearrangement mechanism proposed in the previous paragraph. Namely, after initial elastic region A, stages I and II are active, i.e. stacking faults are sliding leading to plastic deformation and multiplication of the (1-11) twins. The two processes involving stacking faults and twins try to adapt the energy injected by the bending load and their contribution in energy absorption is different. Due to energy gradient, the shear strain can increase and promote formation of new twins with a twin plane rotated orthogonal (in boron carbide, within the orthonormal base of the reciprocal space, the crystalline planes (1-11), (011), and (10-1) of the hexagonal crystal family are equivalent) to the plane of the initial stacking faults and twins (stage III). Some balance is achieved overall, and at macro level the material sustains deformation so that the bending strength is approximately constant for a ductile-type deformation with a relatively large strain as in the deformation region B. When the process of twin rearrangement is almost completed, the new twins in the most stable configuration (stage IV) will block sliding and plastic behavior and strengthening will occur, shifting the bending strength to high values within an elastic-like behavior as recorded in the region C of the strength-strain curves.

The proposed nano scale mechanism of the defects rearrangement in B_4C explains the deformation behavior of the composite and special mechanical response of the composite under bending load at 1800 °C. It is worthy to note that contribution of the TiB_2 grains and of their 3D network is currently unclear and requires further research. In addition, we also observe that bending strength at 2000 °C [25] was higher than in this work attaining in some samples ~8 GPa. In these samples amorphous nano regions were detected. Therefore, expectations are that deformation mechanisms other than those presented in this work can be active in the TiB_2-B_4C composites depending on experimental conditions.

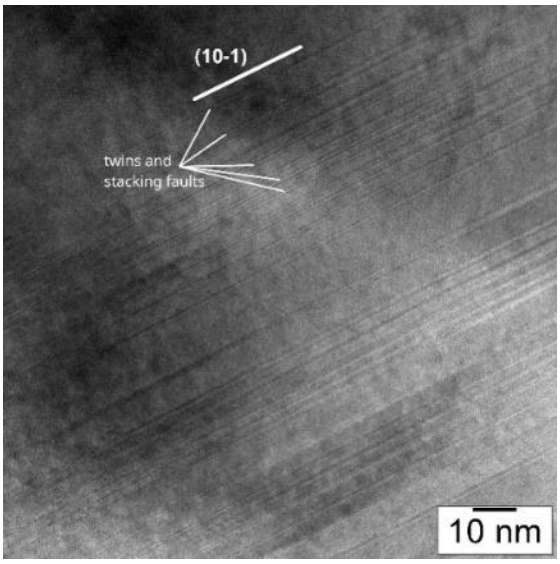

Fig. 4 HRTEM image showing nano-twins and stacking faults in a B_4C grain from the fractured surface after bending the TiB_2-B_4C composite sample at 1800 °C.

3.3 Strenghtening and ductility at high temperatures in high entropy diboride $(Ti_{0.25}Ta_{0.25}Hf_{0.25}Zr_{0.25})B_2$

In Fig. 5 is presented the microstructure at micron scale of the $(Ti_{0.25}Ta_{0.25}Hf_{0.25}Zr_{0.25})B_2$ HEDB. At low magnification (Fig. 5 a) the appearance is uniform and EDS spectrum (Fig. 5 a1) measured on the entire area of the SEM image shows the presence of elements with the ratio of the cations Ti/Ta/Hf/Zr being close to designed one of 1/1/1/1. Nevertheless, at higher magnification (Fig. 5b) one can observe that microstructure resembles a composite of matrix (region 1 in Fig. 5b) and island-like reinforcement (region 2 in Fig. 5b) type. Reinforcement grains (from region 2) are large and in backscattering regime they are brighter suggesting the presence of heavier elements. Indeed, local EDS analysis (Fig 5 c, c1, and c2) indicates that the matrix is roughly Ti-rich and Ta-poor, while the reinforcement is Ti-poor and Ta-rich. The presence of 2 diboride phases with AlB_2 crystal structure is confirmed by X-ray diffraction [22] where diffraction peaks show systematically the presence of a shoulder at higher 2θ diffraction angles, meaning that the crystal structure is the same, but the two phases have different compositions. An average metal composition of the two phases is roughly $Ti_{0.22}Ta_{0.44}Hf_{0.08}Zr_{0.26}$ and $Ti_{0.08}Ta_{0.62}Hf_{0.11}Zr_{0.18}$ from the matrix and the island (reinforcement), respectively. These metal compositions are not balanced and, more important, they cannot support the average metal composition of the material, found to be close to the designed one, as already noted at the beginning of this paragraph. To understand this, we performed a detailed TEM investigation which has shown that at nano scale, the grains are not homogeneous and present a variety of local compositions, while the AlB_2 crystal

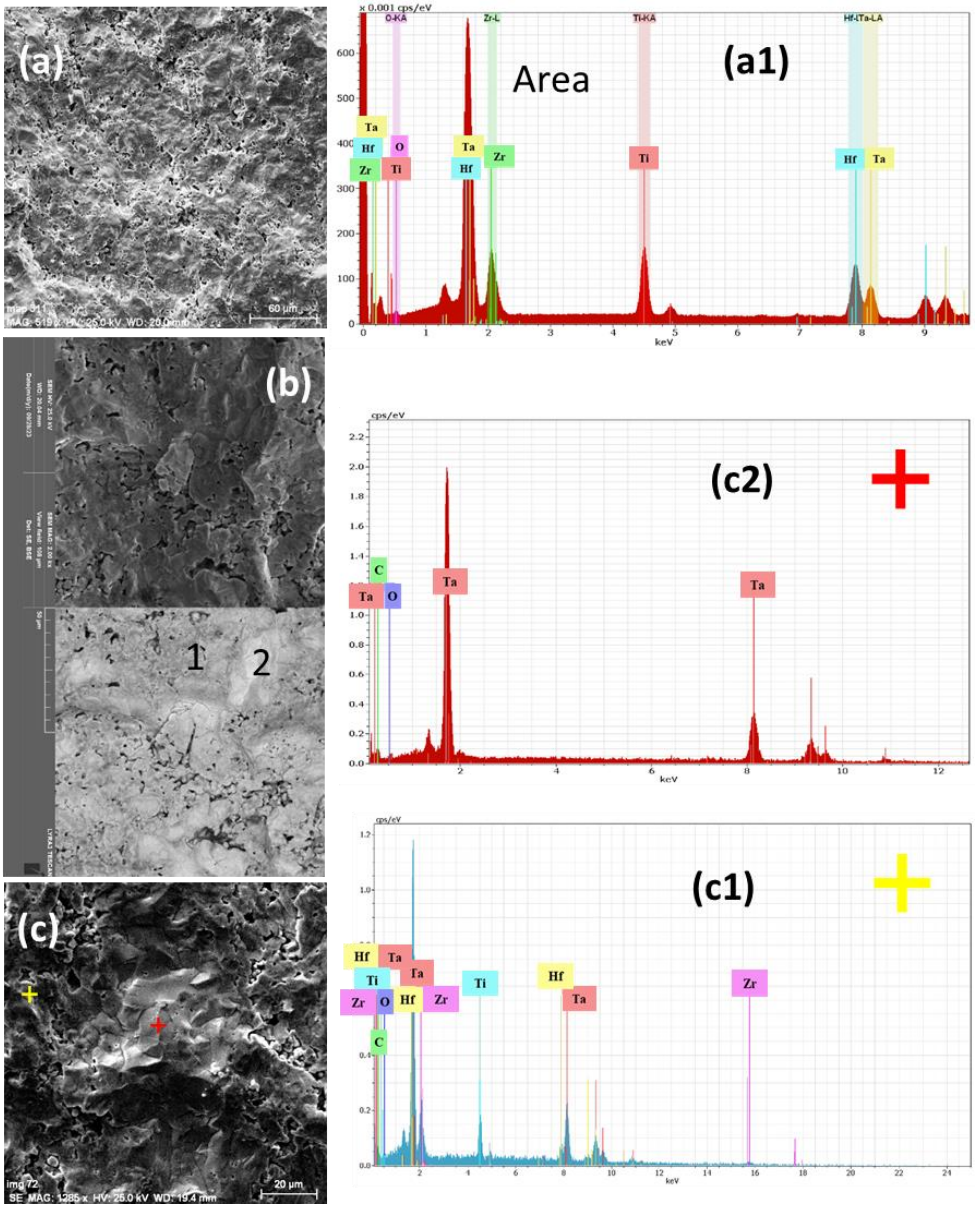

Fig. 5 Microstructure of $(Ti_{0.25}Ta_{0.25}Hf_{0.25}Zr_{0.25})B_2$ observed by SEM: (a)- secondary electrons image taken at low magnification; (a1)- EDS spectrum taken on the full area of the SEM image from (a); (b)- secondary electrons (top) and backscattering electrons (bottom) images taken at a higher magnification; (c) secondary electrons image and local EDS analysis (marked with crosses), spectra being presented in (c1) and (c2).

structure is preserved. In Fig. 6, EDS elemental maps over a grain are not uniform. The interfaces between regions are not sharp and their composition is graded over some distances. The interfaces are also wavy with irregular shapes.

Previous paragraph shows that the microstructure at micro and nano scales of the HEDB is complex. It is heterogeneous and composed on multiple diboride phases with graded and vague interfaces. These aspects make it to stand apart from the composites presented in Sections 3.1 and 3.2. In addition, it does not share the composite microstructure type of 'two interpenetrated 3D networks of the major components" as for MgB_2-hBN, MgB_2-G and TiB_2-B_4C composites. However, after bending at 2000 °C, dislocations were observed [22]. Some of them were protruding from one local compositional region inside a grain to another or from one grain to another, but the density of the dislocations in the neighboring regions or grains was different. From this viewpoint, there is a resemblance with TiB_2-B_4C composite, i.e. mechanical properties at high temperatures of bending are dependent on dislocation behavior, although the mechanisms leading to strengthening and ductility can be different. The HEDB shows a strengthening mechanism without an obvious plastic deformation up to 1800 °C (Fig. 7). After bending at 2000 °C material retains a bending strength that is still higher with ~25 % than the value at RT. In this sample a ductile deformation with a strain of ~7.5 % occurs and at the end of it sample collapses [22].

Literature indicates that small nano-size ceramic samples may present plasticity under compressive load at room temperature. Among them we mention SiC, MgO, diamond and different nano-grained ceramic [26-33]. Crystal chemistry aspects and nano structuring play an important role in mechanical properties and this is also the case of the HEDB. Nevertheless, HEDB successfully extends at a certain temperature mechanical features observed at nano scale to a micro scale.

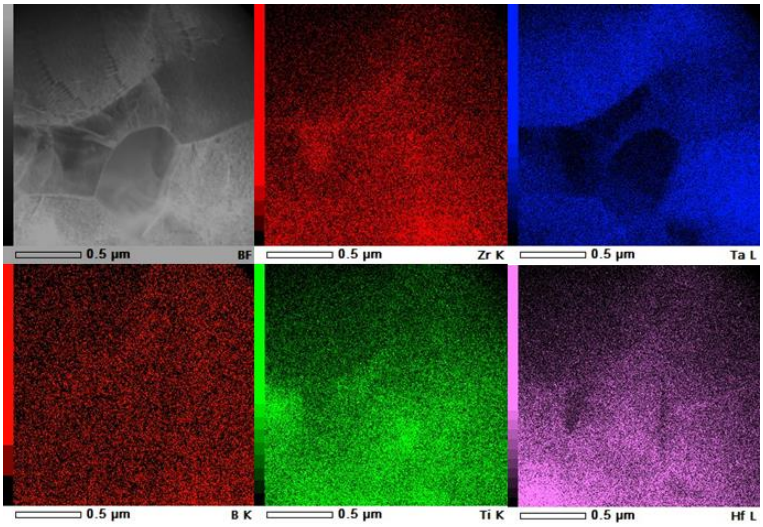

Fig. 6 TEM image and EDS maps of elements Ti, Ta, Hf,, Zr and B taken on $(Ti_{0.25}Ta_{0.25}Hf_{0.25}Zr_{0.25})B_2$ HEDB after bending at 2000 °C.

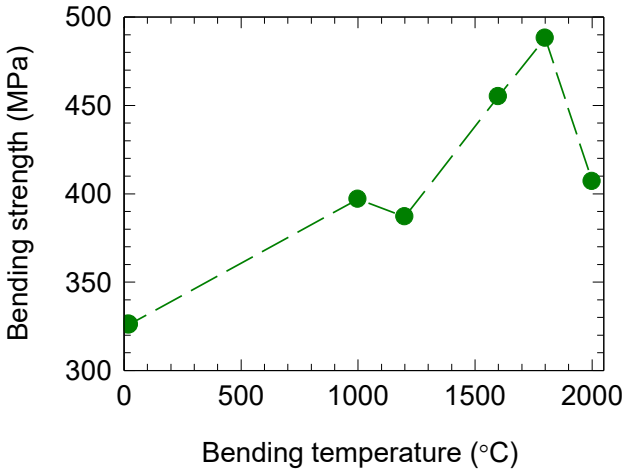

Fig. 7 Ultimate bending strength as a function of bending temperature measured on $(Ti_{0.25}Ta_{0.25}Hf_{0.25}Zr_{0.25})B_2$ HEDB.

4. Conclusion

Comparative analysis of the mechanical properties of the proposed ceramic study cases with complex microstructures suggests that crystal structure details, including defects, along with nanostructuring and microstructuring, are key factors for controlling mechanical properties and overcoming limitations in ductility and strength. The material's response under mechanical load can be counterintuitive; thus, the synergistic contribution of microstructural elements and deformation mechanisms at different scales can lead to unexpected improvements in strength and ductility, occurring simultaneously.

Heterogeneous systems may depart from the conventional definition of a micro or a nano composite where grains are not homogeneous compositionally and they form inside and between grains fuzzy interfaces with graded compositions (e.g., $(Ti_{0.25}Ta_{0.25}Hf_{0.25}Zr_{0.25})B_2$ HEDB). This type of system leverages the specifics of solid-state reaction routes, which are the main approaches of powder metallurgy, making their heterogeneous microstructures difficult to achieve through casting technologies. Heterogeneous systems are expected to exhibit not only excellent mechanical properties, but also other characteristics: in this work, a machinable, chip-friendly ceramic-like MgB_2-based superconductor was demonstrated to have potential for bulk superconducting magnet applications.

The work emphasizes that controlling microstructure at different scales—nanoscale, microscale, and macroscale—is essential to tailor mechanical and other properties. However, the principles and criteria for designing materials that combine strength and ductility are not yet fully established. Moreover, scaling up many outstanding properties observed at the nano level, including mechanical ones,

remains a challenge. The interaction between system components, such as in the TiB_2-B_4C composite, presents difficulties in understanding and stays unclear.
It is noteworthy that the materials studied in this work present exceptional mechanical properties without requiring an excessively large number of elements: the maximum number of elements in this work is 5 as for $(Ti_{0.25}Ta_{0.25}Hf_{0.25}Zr_{0.25})B_2$ HEDB.

Acknowledgements

P.B., M.-A.G., A.K. G.A, and M.B. acknowledge financial support from UEFISCDI Romania through Core Program PC2-PN23080202 and PN-IV-P1-PCE-2023-1692 (CCOS). O.V. acknowledges the support of the JSPS KAKENHI Grants-in-Aid for Scientific Research (24K08035).

References

[1] Tiwary C. S., Pandey P., Sarkar S., Das R., Samal S., Biswas K., Chattopadhyay K., *Five decades of research on the development of eutectic as engineering materials*, Progress in Materials Science, **123**, 2022, p. 100793.
[2] Ritchie O. R., *The conflicts between strength and toughness*, Nature Materials, **10**, 2011, p. 817-822.
[3] Valiev R.Z., Alexandrov I.V., Zhu Y.T., Lowe T.C., *Paradox of strength and ductility in metals processed by severe plastic deformation*, J. Mater. Res., **17**, 2002, p. 5-8.
[4] Ma E., Zhu T., *Towards strength-ductility synergy through the design of heterogeneous nanostructures in metals*, Mater. Today, **20**, 2017, p. 323-331.
[5] Wang Y. M., Ma E., *Three strategies to achieve uniform tensile deformation in a nanostructured metal*, Acta Mater., **52**, 2004, p.1699-1709.
[6] Tsakiropoulos P., *Alloys for application at ultra-high temperatures: Nb-silicide in situ composites: Challenges, breakthroughs and opportunities*, Progress in Materials Science, **123**, 2022, p. 100714.
[7] Cantor B., Chang I. T. H., Knight P., Vincent A. J. B., *Microstructural development in equiatomic multicomponent alloys*, Mater. Sci. Eng.:A, **375-377**, 2004, p. 213-218.
[8] Sathiyamoorthi P., Asghari-Rad P., Bae J. W., Kim H. S., *Fine tuning of tensile properties in CrCoNi medium entropy alloy through cold rolling and annealing*, Intermetallics, **113**, 2019, p. 106578.
[9] Bae J.W., Moon J., Jang M.J., Yim D., Kim D., Lee S., Kim H. S., *Trade-off between tensile property and formability by partial recrystallization of CrMnFeCoNi high entropy alloy*, Mater. Sci. Eng. A, **703**, 2017, p.324-330.
[10] Wu X., Yang M., Yuan F., Wu G., Wei Y., Huang X, Zhu Y., *Heterogeneous lamella structure unites ultrafine-grain strength with coarse-grain ductility*, Proc. Natl. Acad. Sci. U S A, **112**, 2015, p. 14501-5.
[11] Sathiyamoorthi P., Kim H. S., *High-entropy alloys with heterogeneous microstructure: Processing and mechanical properties*, Progress in Materials Science, **123**, 2022, p. 100709.
[12] Huang L. J., Geng, L., Peng, X.-X., *Microstructurally inhomogenous composites: Is a homogenous reinforcement distribution optimal?*, Prog. Mater. Sci., **71**, 2015, p. 93-168.
[13] Fediuk R. S., Yevdokimova Yu G., Smoliakov A. K., Stoyushko Yu N., Lesovik V. S., *Use of geonics scientific positions for designing of building composites for protective (fortification) structures*, IOP Conf. Ser.: Mater. Sci. Eng., **221**, 2017, p. 012011.
[14] Marthin O., Gamstedt E. K., *Damage shielding mechanisms in hierarchical composites in nature with potential for design of tougher structural materials*, R. Soc. open sci., **6**, 2023, p. 181733.

[15] Barthelat F., Rabiei R., *Toughness amplification in natural composites*, Journal of the Mechanics and Physics of Solids, **59**, 2011, p. 829.
[16] Nagamatsu J., Nakagawa N., Muranaka T., Zenitani Y., Akimitsu J., Superconductivity at 39 K in magnesium diboride, Nature, **410**, 2001, p. 63-64.
[17] Badica P., Batalu D., *Beyond superconductivity towards novel biomedical, energy, ecology, and heritage applications of MgB_2*, Green Chemistry Letters And Reviews, **15**, 2022, p. 646-657.
[18] Aldica G.V., Burdusel M., Cioca E.M., Badica P., *Machinable superconducting material and magnetic field concentrator/storer made of a superconducting material based on MgB_2, machinable by chip removal*, RO130252-B1, 2020.
[19] Aldica G.V., Burdusel M., Badica P., *Method of manufacturing machinable superconducting material and magnetic field concentrator/storer involves, mixing the powder.* RO131791-B1, 2021.
[20] Burdusel M., Aldica G. V., Pasuk I., Grigoroscuta M. A., Kuncser A., Badica P., *Trapped Magnetic Field of MgB_2 Machinable Disks with Diferent*, Additives, Journal of Superconductivity and Novel Magnetism, **38**, 2025, p. 179.
[21] Kuncser A., Vasylkiv O., Borodianska H., Demirskyi D., Badica P., *High bending strength at 1800 °C exceeding 1 GPa in TiB_2-B_4C composite*, Scientific Reports, **13**, 2023, p. 6915.
[22] Badica P., Grigoroscuta M. A., Kuncser A. Cristian., Vasylkiv O., *High-Entropy Ti, Zr, Hf, Ta Multiphase Diboride with Deformation Resistance up to* 2000 °C, Adv. Eng. Mater., **27**, 2025, p. 2402723.
[23] Badica P., Aldica G., Burdusel M., Popa S., Negrea R. F., Enculescu M., Pasuk I., Miu L., *Significant enhancement of the critical current density for cubic BN addition into ex situ spark plasma sintered MgB_2*, Supercond. Sci. Technol., **27**, 2014, p. 095013.
[24] Aldica G., Burdusel M., Popa S., Hayasaka Y., Badica P., *Graphene addition to MgB_2 superconductor obtained by ex-situ spark plasma sintering technique*, Mater. Res. Bull. **77**, 2016, p. 205-211.
[25] Demirskyi D., Sepehri-Amin H., Suzuki T. S., Vasylkiv O., *Ultra-high temperature texure and strain driven amorphization in polycrystalline boron carbide bulks*, Scripta Mater., **210**, 2022, p. 114487.
[26] Amodeo J., Merkel S., Tromas C., Carrez P., Korte-Kerzel S., Cordier P., Chevalier J., *Dislocations and Plastic Deformation in MgO Crystals: A Review*, Crystals, **8**, 2018, p. 240.
[27] Nie A., Bu Y., Huang J., Shao Y., Zhang Y., Hu W., Liu J., Wang Y., Xu Bu, Liu Z., Wang H., Yang W., Tian Y., *Direct Observation of Room-Temperature Dislocation Plasticity in Diamond*, /Matter, **2**, 2020, p. 1079–1090.
[28] Jiang B., Weng G. J., *A theory of compressive yield strength of nano-grained ceramics*, Int. J. Plast., **20**, 2004, p. 2007-2026.
[29] Wang F., Yan X., Zhang C., Deng L., Lu Y., Nastasi M., Cui B., *Localized plasticity in silicon carbide ceramics induced by laser shock processing*, Materialia, **6**, 2019, p. 100265.
[30] Shen C., Li J., Niu T., Cho J., Shang Z., Zhang Y., Shang A., Yang B., Xu K., García R. E., Wang H., Zhang X., *Achieving room temperature plasticity in brittle ceramics through elevated temperature preloading*, Sci. Adv., **10**, 2024, p. eadj4079.
[31] Östlund F., Rzepiejewska-Malyska K., Leifer K., Hale L. M., Tang Y., Ballarini R., Gerberich W. W., *Michler, Brittle-to-Ductile Transition in Uniaxial Compression of Silicon Pillars at Room Temperature*, J. Adv. Funct. Mater, **19**, 2009, p. 2439.
[32] Michler J., Wasmer K., Meier S., Östlund F., Leifer K., *Plastic deformation of gallium arsenide micropillars under uniaxial compression at room temperature*, Appl. Phys. Lett., **90**, 2007, p. 043123.
[33] Kiani S., Ratsch C., A. Minor M., Kodambaka S., Yang J.-M., *Orientation- and size-dependent room-temperature plasticity in ZrC crystals*, Phil. Mag., **95**, 2015, p. 985-997.